Geostatistical inverse modeling of transient pumping tests using temporal moments of drawdown

Wei Li

Swiss Federal Institute of Aquatic Science and Technology (EAWAG), Dübendorf, Switzerland

Wolfgang Nowak

Institut für Wasserbau, Universität Stuttgart, Stuttgart, Germany

Olaf A. Cirpka

Swiss Federal Institute of Aquatic Science and Technology (EAWAG), Dübendorf, Switzerland

[1] Pumping tests belong to the most common techniques of hydrogeological site assessment. While the steady state drawdown is determined by the distribution of transmissivity alone, the transient behavior is also influenced by the storativity field. In geostatistical inverse modeling the spatial distributions of both transmissivity and storativity are inferred from the drawdown curves and prior information on the spatial correlation of the parameter fields. So far, however, transient data have hardly been analyzed by geostatistical inverse methods because the computational effort is rather high. In the present study, we characterize the drawdown by its temporal moments. We present moment-generating equations and corresponding equations to compute the sensitivity of the temporal moments of drawdown with respect to the distributions of transmissivity and storativity. We utilize these equations to infer the transmissivity and storativity fields from transient pumping tests using the quasi-linear geostatistical approach of inverse modeling. Considering temporal moments rather than full drawdown curves drastically reduces the computational effort of the estimation procedure. In test cases we show that the first two temporal moments are sufficient to characterize the drawdown curves. We investigate how erroneous assumptions regarding the spatial variability of storativity affect the estimate of the transmissivity field, and we analyze the effect of truncating the measured drawdown curves.

1. Introduction

[2] Accurate predictions of flow and transport in geological formations require detailed knowledge about the spatial distribution of hydrogeological parameters, such as the hydraulic conductivity and the specific storage coefficient. Among the most common techniques for hydrogeological site investigation are pumping tests, in which water is extracted from a production well and the drawdown is monitored in adjacent monitoring wells [e.g., *Kruseman and de Ridder*, 1991]. At steady state, the drawdown depends only on boundary conditions and the distribution of transmissivity. The transient behavior, by contrast, is also sensitive to the storativity of the formation.

[3] Conventional analyses of pumping tests yield effective values of the transmissivity T and the storage coefficient S by fitting analytical solutions to measurements of drawdown [e.g., *Kruseman and de Ridder*, 1991]. The analytical expressions have been derived for infinite domains with uniform conditions. The parameters determined are average properties of the aquifer over a large volume [e.g., *Butler and Liu*, 1993; *Oliver*, 1993]. *Sanchez-Vila et al.* [1999] showed that the transmissivities, determined by Jacob's method from single observation wells in transient pumping tests, approach the effective transmissivity of the formation, whereas the estimated storativities differ strongly between the various observation wells. *Neuman et al.* [2004] derived a type curve method for steady state pumping tests, in which geostatistical parameters of the formation are retrieved from the variation of drawdown profiles. The type curve approaches, however, do not resolve the spatial distributions of transmissivity T and storativity S. At most, they yield a mean value and statistical parameters regarding the spatial variability.

[4] Pumping test data have been analyzed with parameter estimation schemes coupled to numerical groundwater flow models [e.g., *Barrash and Dougherty*, 1997; *Thorbjarnarson et al.*, 1998]. In the latter studies, definite structures of the subsurface, e.g., layers with known thickness or zones of well-known geometry, were assumed and uniform parameters within each structure were determined by minimizing the sum of weighted squared errors. The principal difficulty

with this type of inverse models is that the deterministic structure of the aquifer must be known a priori.

[5] In contrast to deterministic models, geostatistical inverse methods impose minimum prior information about the spatial distribution of parameters [e.g., *Hoeksema and Kitanidis*, 1984; *Rubin and Dagan*, 1987; *Kitanidis*, 1995; *Mclaughlin and Townley*, 1996; *Yeh et al.*, 1996; *Zimmerman et al.*, 1998]. Here, the hydraulic parameters are allowed to vary continuously throughout the domain, and the prior information is limited to the covariance function of parameter fluctuations and the structure of a trend model. The approach of Kitanidis and various co-workers [e.g., *Hoeksema and Kitanidis*, 1984; *Kitanidis*, 1995] even allows inferring the structural parameters of the covariance function from the data.

[6] Like many inverse methods, the geostatistical approach requires computing the sensitivity of all measured quantities with respect to the log transmissivity at each point within the domain. These computations are performed most efficiently by the adjoint state method [e.g., *Sun and Yeh*, 1990], in which only a single adjoint partial differential equation per observation point has to be solved.

[7] *Sun and Yeh* [1992] presented a geostatistical inverse method to identify the transmissivity under transient groundwater flow conditions. *Yeh* [1992] discussed applications of the method to transient pumping tests. The approach requires computing cross-covariance functions between log transmissivity and hydraulic head at all observation times. Thus the computational efficiency of the adjoint state method is counteracted by the number of observation points in time. Recently, *Zhu and Yeh* [2005] showed that only a few measurement points in time need to be considered in inverse modeling because the transient heads at a given location are strongly correlated in time. Other geostatistical inverse methods, such as the pilot point method [*Certes and de Marsily*, 1991] and the method of sequential self calibration [*Hendricks Franssen et al.*, 1999], do not rely on cross-covariance matrices and are more efficient in handling transient data. However, they still require repeatedly computing multiple time steps.

[8] As a computationally efficient alternative to solving the standard transient groundwater flow equation, a group of authors has transferred ray-tracing techniques, derived in seismic tomography, to the analysis of transient head data [*DattaGupta et al.*, 1997; *Vasco et al.*, 2000; *Brauchler et al.*, 2003; *Vasco and Finsterle*, 2004]. Here, the propagation of pressure waves is computed along trajectories. That is, the original parabolic equation is replaced by an asymptotic hyperbolic equation, for which efficient particle-tracking-like techniques can be used. On the basis of the solution of the asymptotic equation, an inverse modeling technique has been developed, in which the ratio of transmissivity over storativity can be determined.

[9] In the present study, we suggest a different approach to reduce the computational effort associated with the geostatistical analysis of transient pumping test data. Rather than directly using pressure heads during transient flow, we consider the temporal moments of drawdown. For a unit pulse extraction, the zeroth temporal moment depends on the transmissivity distribution only, whereas all higher moments also depend on the distribution of storativity. In section 2, we derive moment-generating equations that are formally equivalent to steady state flow equations with distributed sources. In contrast to the hyperbolic equations of *Vasco et al.* [2000], our elliptic equations are exact. Also, we need not compute trajectories of pressure waves, which by themselves depend on the pressure field.

[10] The concept of moment-generating equations has been introduced to subsurface hydrology by *Harvey and Gorelick* [1995b], who analyzed solute transport of kinetically sorbing compounds. Temporal moments have been used in geostatistical inverse models by *Harvey and Gorelick* [1995a], *James et al.* [2000], and *Cirpka and Kitanidis* [2000]. In these studies, the moments of tracer data were used, while we consider here those of head-related quantities. The main advantage in both applications is the same: a transient equation is replaced by a series of steady state equations.

[11] While a pulse-like injection of tracer may reflect experimental conditions of a tracer test, it is uncommon to extract only a single pulse of water in a pumping test. Thus we present how the pulse-related moments correspond to quantities that can be measured in a pumping test with continuous extraction or extraction over a time period.

[12] We combine the method to compute temporal moments of drawdown with the quasi-linear geostatistical approach of inverse modeling [*Kitanidis*, 1995], which minimizes the likelihood of the parameters, given observations of dependent quantities. The prior knowledge about the parameters is restricted to uncertain drift coefficients and a covariance function for the fluctuations about the trend. In our implementation, the method is accelerated by the continuous adjoint state method to compute sensitivities [*Sun and Yeh*, 1990], and spectral methods to compute the cross covariances between drawdown moments and the hydraulic parameters [*Nowak et al.*, 2003]. We stabilize the method by a modified Levenberg-Marquardt approach [*Nowak and Cirpka*, 2004]. The inverse procedure and the evaluation of sensitivities are briefly described in sections 3 and 4, whereas sections 5 and 6 contain applications to hypothetical test cases and discuss some properties of the estimated parameter fields.

2. Governing Equations

[13] In this section, we present moment-generating equations for drawdown and demonstrate how transient data from pumping tests relate to the temporal moments of a pumping test with unit pulse extraction.

2.1. Transient Drawdown in Confined Aquifers

[14] Consider regional, depth-integrated flow in a confined aquifer. Prior to the pumping test, the system is assumed to be in steady state. Over the time period of the test, the boundary conditions, except for the pumping, do not change. Then, we can define the drawdown s (m):

$$s(\mathbf{x}, t) = h(\mathbf{x}, t_0) - h(\mathbf{x}, t), \tag{1}$$

in which $h(\mathbf{x},t)$ (m) is the hydraulic head at location $\mathbf{x}$ (m) and time t [s], whereas t_0 [s] is the time at which pumping starts. The drawdown meets the following parabolic partial differential equation:

$$S\frac{\partial s}{\partial t} - \nabla \cdot (T\nabla s) = Q(t)\delta(\mathbf{x} - \mathbf{x}_w), \tag{2}$$

A: Pulse–Like Extraction

B: Extraction over Time Period
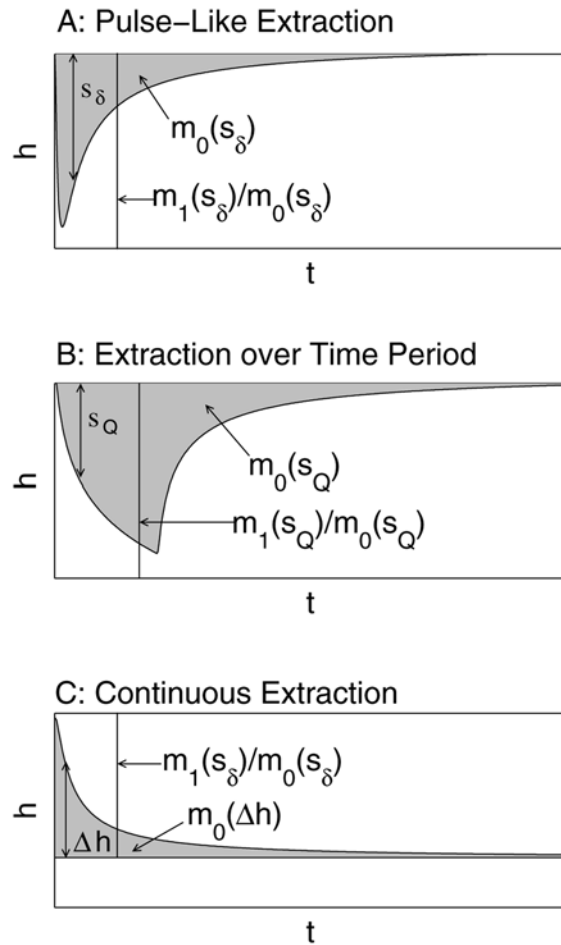

C: Continuous Extraction

Figure 1. Transient hydraulic heads in a pumping test as function of time for various regimes of extraction.

with the initial and boundary conditions:

$$s = 0 \quad \text{at} \quad t = t_0, \tag{3}$$

$$s = 0 \quad \text{on} \quad \Gamma_{Diri} \forall t, \tag{4}$$

$$\mathbf{n} \cdot \nabla s = 0 \quad \text{on} \quad \Gamma_{Neu} \forall t, \tag{5}$$

in which the depth-integrated coefficients S (dimensionless) and T (m^2/s) are the storativity and transmissivity, $Q(t)$ (m^3/s) is the pumping rate, $\delta(\mathbf{x} - \mathbf{x}_w)$ (1/m^2) is the Dirac delta function, $\mathbf{x}_w$ (m) is the location of the well, Γ_{Diri} and Γ_{Neu} denote Dirichlet and Neumann boundaries, and $\mathbf{n}$ (dimensionless) is the unit vector normal to the boundaries.

[15] In practice, we conduct a pumping test either by extracting water with a rate $Q(t)$ over a finite period of time, or by pumping with a constant rate Q until steady state is reached. Because of the linearity of equation (2), the drawdown $s_Q(\mathbf{x}, t)$ for an arbitrary pumping regime $Q(t)$ can be computed from the drawdown $s_\delta(\mathbf{x}, t)$ (s/m^2), valid for instantaneous extraction of a unit volume, by convolution

$$s_Q(\mathbf{x}, t) = \int_0^t s_\delta(\mathbf{x}, t - \tau) Q(\tau) d\tau. \tag{6}$$

[16] For the case of continuous extraction, i.e., $Q(t) = Q$, we consider the steady state drawdown $s_\infty(\mathbf{x}) = Q \int_0^\infty s_\delta(\mathbf{x}, \tau) d\tau$, and the deviation from the steady state drawdown $\Delta h(\mathbf{x}, t) = s_\infty(\mathbf{x}) - s(\mathbf{x}, t) = Q \int_t^\infty s_\delta(\mathbf{x}, \tau) d\tau$.

[17] Figure 1 shows the transient head curves for pumping tests with pulse-like extraction (Figure 1a), extraction over a time period (Figure 1b), and continuous extraction (Figure 1c). In the following, we will discuss how to characterize these curves by temporal moments and how the moments of the cases in Figures 1b and 1c are related to those of the case in Figure 1a.

2.2. Temporal Moments of Drawdown

[18] We characterize the transient behavior of the drawdown $s(\mathbf{x}, t)$ by its temporal moments. The kth moment $m_k(s(\mathbf{x}))$ [ms^{k+1}] is defined by

$$m_k(s(\mathbf{x})) = \int_0^\infty t^k s(\mathbf{x}, t) dt. \tag{7}$$

[19] In this study, we consider the zeroth moment $m_0(s(\mathbf{x}))$ and the first moment $m_1(s(\mathbf{x}))$. For a unit pulse extraction, the zeroth moment corresponds to the steady state drawdown of a corresponding pumping test with continuous extraction, whereas the normalized first moment $m_1(s(\mathbf{x}))/m_0(s(\mathbf{x}))$ is a characteristic time of drawdown.

[20] The moments of the unit pulse response $s_\delta(\mathbf{x}, t)$ are related to those of the drawdown $s_Q(\mathbf{x}, t)$ due to extraction $Q(t)$ over a time period by

$$m_0(s_\delta(\mathbf{x})) = \frac{m_0(s_Q(\mathbf{x}))}{m_0(Q)}, \tag{8}$$

$$\frac{m_1(s_\delta(\mathbf{x}))}{m_0(s_\delta(\mathbf{x}))} = \frac{m_1(s_Q(\mathbf{x}))}{m_0(s_Q(\mathbf{x}))} - \frac{m_1(Q)}{m_0(Q)}, \tag{9}$$

whereas the moments of $s_\delta(\mathbf{x}, t)$ can be computed from quantities of continuous extraction by:

$$m_0(s_\delta(\mathbf{x})) = \frac{s_\infty(\mathbf{x})}{Q}, \tag{10}$$

$$\frac{m_1(s_\delta(\mathbf{x}))}{m_0(s_\delta(\mathbf{x}))} = \frac{m_0(\Delta h(\mathbf{x}))}{s_\infty(\mathbf{x})}. \tag{11}$$

[21] In Figure 1, zeroth moments are marked as shaded areas, and characteristic times m_1/m_0 by vertical lines. For the cases of a pulse-like extraction and an extraction over a time period, the characteristic times are the centers of gravity of the shaded areas.

[22] Because of the identities given above, it is clear that the zeroth and first moments for unit pulse extraction, $m_0(s_\delta(\mathbf{x}))$ and $m_1(s_\delta(\mathbf{x}))$, can be computed for any type of pumping regime occurring in practical applications.

2.3. Moment-Generating Equations

[23] *Harvey and Gorelick* [1995b] derived moment-generating equations for the transport of sorbing solutes using the Laplace transform of the transport equation. Here

we derive the moment-generating equations for drawdown s_δ due to unit pulse extraction, without applying the Laplace transformation. In order to compute the kth moment, we multiply equation (2) with t^k, integrate over time, apply rules of partial integration to the term with the time derivative, and consider the initial condition, equation (3). For $Q(t) = \delta(t)$, we arrive at

$$-\nabla \cdot (T\nabla m_k) = \delta_{k0}\delta(\mathbf{x} - \mathbf{x}_w) + kSm_{k-1}. \qquad (12)$$

Here, δ_{k0} is the Kronecker delta, which is unity for $k = 0$ and zero otherwise. The boundary conditions are obtained by multiplying equations (4) and (5) with t^k and integrating over time:

$$m_k = 0 \quad \text{on} \quad \Gamma_{Diri}\forall t, \qquad (13)$$

$$\mathbf{n} \cdot \nabla m_k = 0 \quad \text{on} \quad \Gamma_{Neu}\forall t. \qquad (14)$$

[24] The equation generating the zeroth moment $m_0(s_\delta(\mathbf{x}))$, equation (12) with $k = 0$, is a steady state groundwater flow equation with an extraction rate of unity at the well location. It does not depend on the storativity S. Because we consider the normalized case of a unit pulse, $m_0(s_\delta(\mathbf{x}))$ neither depends on the pumping rate. By contrast, the moment-generating equations for the higher-order moments $m_{k>0}(s_\delta(\mathbf{x}))$, equation (12) with $k > 0$, are steady state flow equations with a distributed rather than a point-like source. The distributed source term is proportional to the next lower-order moment $m_{k-1}(s_\delta(\mathbf{x}))$ and the storativity $S(\mathbf{x})$. Therefore the zeroth moment $m_0(s_\delta(\mathbf{x}))$ can be used to infer the distribution of transmissivity $T(\mathbf{x})$, whereas at least the zeroth and first moments, $m_0(s_\delta(\mathbf{x}))$ and $m_1(s_\delta(\mathbf{x}))$, are needed to jointly estimate the storativity $S(\mathbf{x})$.

[25] By applying moment-generating equations, we transfer the transient groundwater flow problem into a steady state framework. In this paper, we use the two most important and characteristic temporal moments, i.e., the zeroth and first moments, to characterize drawdown curves. For given parameter distributions, they are computed by solving two elliptic equations. In comparison to solving for transient hydraulic heads in multiple time steps, we thus drastically reduce the computational costs.

3. Geostatistical Inverse Method

[26] We identify the unknown distributions of log transmissivity $Y = \ln(T)$ and log storativity $Z = \ln(S)$ following the quasi-linear geostatistical approach of *Kitanidis* [1995], which finds the peak of the conditional probability density function of the parameters $\mathbf{p}$, given the measurements $\mathbf{m}$. We consider uncertain prior knowledge of the trend coefficients describing the mean values of the parameters. In this section, we briefly review the inverse approach.

[27] We discretize the domain into n_Y elements. For each element, we assume an element-wise uniform log transmissivity Y_i and a log storativity value Z_i. Thus the set of all values for Y_i and Z_i forms the $(2n_Y \times 1)$ vector $\mathbf{p}$ of parameters. We consider $\mathbf{p}$ to be random, drawn from a multi-Gaussian distribution with expected value $E[\mathbf{p}|\boldsymbol{\beta}] = \mathbf{X}\boldsymbol{\beta}$ and covariance matrix $\mathbf{C_{pp}}$: $\mathbf{p} \sim N(\mathbf{X}\boldsymbol{\beta},\mathbf{C_{pp}})$. Here, $\mathbf{X}$ is a $(2n_Y \times n_\beta)$ matrix of known base functions, and $\boldsymbol{\beta}$ is a $(n_\beta \times 1)$ vector of uncertain drift coefficients.

The prior knowledge of $\boldsymbol{\beta}$ is quantified by a multi-Gaussian distribution with prior mean $\boldsymbol{\beta}^*$ and covariance matrix $\mathbf{C_{\beta\beta}}$: $\boldsymbol{\beta} \sim N(\boldsymbol{\beta}^*, \mathbf{C_{\beta\beta}})$. Then, $\mathbf{p}$ is distributed: $\mathbf{p} \sim N(\mathbf{X}\boldsymbol{\beta}^*,\mathbf{G_{pp}})$, where $\mathbf{G_{pp}} = \mathbf{C_{pp}} + \mathbf{X}\mathbf{Q_{\beta\beta}}\mathbf{X^T}$ is the $(2n_Y \times 2n_Y)$ generalized autocovariance matrix of $\mathbf{p}$, whereas $\mathbf{C_{pp}}$ is the covariance of $\mathbf{p}$ given $\boldsymbol{\beta}$. If the log transmissivity $Y(\mathbf{x})$ and the log storativity $Z(\mathbf{x})$ are assumed uncorrelated, the parameter vector $\mathbf{p}$, the drift function $\mathbf{X}$, the vector of drift coefficients $\boldsymbol{\beta}$, and the covariance matrix of parameters $\mathbf{C_{pp}}$ are aggregated from the corresponding quantities for log transmissivity and log storativity by

$$\mathbf{p} = \begin{bmatrix} \mathbf{Y} \\ \mathbf{Z} \end{bmatrix}, \quad \mathbf{X} = \begin{bmatrix} \mathbf{X_Y} & \mathbf{0} \\ \mathbf{0} & \mathbf{X_Z} \end{bmatrix},$$

$$\boldsymbol{\beta} = \begin{bmatrix} \boldsymbol{\beta}_Y \\ \boldsymbol{\beta}_Z \end{bmatrix}, \quad \mathbf{C_{pp}} = \begin{bmatrix} \mathbf{C_{YY}} & \mathbf{0} \\ \mathbf{0} & \mathbf{C_{ZZ}} \end{bmatrix}.$$

[28] The $(n_{obs} \times 1)$ vector of observations $\mathbf{m}$ consists of measured zeroth and first moments of drawdown at the locations of observation. It is related to the parameters $\mathbf{p}$ via a nonlinear transfer function $\mathbf{f}$: $\mathbf{y} = \mathbf{f}(\mathbf{p}) + \mathbf{r}$, in which $\mathbf{r}$ is the $(n_{obs} \times 1)$ vector of observation error with zero mean and the $(n_{obs} \times n_{obs})$ covariance matrix $\mathbf{R}$. In the quasi-linear approach, the transfer function is linearized about the current estimate $\mathbf{p}_k$:

$$\mathbf{f}(\mathbf{p}) \approx \mathbf{f}(\mathbf{p}_k) + \mathbf{H}_k\mathbf{p} - \mathbf{H}_k\mathbf{p}_k, \qquad (15)$$

in which $\mathbf{H}_k$ is the $(n_{obs} \times 2n_Y)$ sensitivity matrix with entries $H_{ij} = \partial f_i(\mathbf{p})/\partial p_j$, derived about the current estimate $\mathbf{p}_k$, and k is the iteration index. For convenience, we define a modified vector of observations $\mathbf{m}'_k$:

$$\mathbf{m}'_k = \mathbf{m} - \mathbf{f}(\mathbf{p}_k) + \mathbf{H}_k\mathbf{p}_k. \qquad (16)$$

[29] Linearized uncertainty propagation yields that $\mathbf{m}'_k \sim N(\mathbf{H}_k\mathbf{X}\boldsymbol{\beta}^*, \mathbf{G}_{\mathbf{mm},k})$, in which $\mathbf{G}_{\mathbf{mm},k} = \mathbf{H}_k\mathbf{G_{pp}}\mathbf{H}_k^T + \mathbf{R}$ is the $(n_{obs} \times n_{obs})$ generalized autocovariance matrix of $\mathbf{m}'_k$.

[30] On the basis of the current linearization, the conditional mean of the parameters $\mathbf{p}_{k+1}$, given the measurements $\mathbf{m}$, is defined by

$$\mathbf{p}_{k+1} = \mathbf{X}\boldsymbol{\beta}_{k+1} + \mathbf{C_{pp}}\mathbf{H}_k^T\boldsymbol{\xi}_{k+1}, \qquad (17)$$

in which the $(n_\beta \times 1)$ vector $\boldsymbol{\beta}_{k+1}$ of conditional drift coefficients and the $(n_{obs} \times 1)$ vector $\boldsymbol{\xi}_{k+1}$ of weights are the solution of the system

$$\begin{bmatrix} \mathbf{H}_k\mathbf{C_{pp}}\mathbf{H}_k^T + \mathbf{R} & \mathbf{H}_k\mathbf{X} \\ \mathbf{X}^T\mathbf{H}_k^T & -\mathbf{C_{\beta\beta}^{-1}} \end{bmatrix} \begin{bmatrix} \boldsymbol{\xi}_{k+1} \\ \boldsymbol{\beta}_{k+1} \end{bmatrix} = \begin{bmatrix} \mathbf{m}'_k \\ -\mathbf{C_{\beta\beta}^{-1}}(\boldsymbol{\beta}^* - \boldsymbol{\beta}_k) \end{bmatrix}. \qquad (18)$$

[31] Conceptually, the quasi-linear approach [*Kitanidis*, 1995] consists of a single Bayesian updating step, in which all measurements are accounted for at once. The iterations are needed only to obtain the sensitivity about the posterior rather than the prior parameter vector. This is different to the approach of *Yeh et al.* [1996] and *Zhu and Yeh* [2005], where the measurements are introduced sequentially in a series of Bayesian updating steps.

[32] In the original quasi-linear approach [*Kitanidis*, 1995], the iterative procedure consisted of the following steps: (1) evaluation of the forward model using the current estimate, (2) derivation of the sensitivities about the estimate, (3) update of the parameters $\mathbf{p}_{k+1}$ according to equation (17) using the modified measurement vector $\mathbf{m}'_k$ according to equation (16) and the drift coefficients $\boldsymbol{\beta}_{k+1}$ and weights $\boldsymbol{\xi}_{k+1}$ computed by equation (18). This procedure was repeated until a convergence criterion was met. In cases of high variability, unfortunately, the original scheme may become instable, that is, the updated parameter vector may not approach a unique solution. Therefore we stabilize the scheme by a modification of the Levenberg-Marquardt algorithm as described by *Nowak and Cirpka* [2004]. Also, we evaluate the terms $\mathbf{H}_k\mathbf{C}_{\mathbf{pp}}\mathbf{H}_k^T$ and $\mathbf{C}_{\mathbf{pp}}\mathbf{H}_k^T$, appearing in equations (17) and (18) using periodic embedding and spectral methods [*Nowak et al.*, 2003].

[33] Once the scheme has converged, the conditional covariance matrix $\mathbf{C}_{\mathbf{pp|m}}$ of the parameters $\mathbf{p}$ given the observations $\mathbf{m}$ is computed by

$$\mathbf{C}_{\mathbf{pp|m}} \geq \mathbf{C}_{\mathbf{pp}} - \begin{bmatrix} \mathbf{HC}_{\mathbf{pp}} \\ \mathbf{X}^T \end{bmatrix}^T \begin{bmatrix} \mathbf{HC}_{\mathbf{pp}}\mathbf{H}^T + \mathbf{R} & \mathbf{HX} \\ \mathbf{X}^T\mathbf{H}^T & -\mathbf{C}_{\beta\beta}^{-1} \end{bmatrix}^{-1} \begin{bmatrix} \mathbf{HC}_{\mathbf{pp}} \\ \mathbf{X}^T \end{bmatrix}, \tag{19}$$

in which we have dropped the iteration index, and $\mathbf{H}$ is derived about the posterior mean of the parameter vector $\mathbf{p}$.

4. Evaluation of Sensitivities

[34] In the quasi-linear geostatistical approach of inverse modeling, we repeatedly need to evaluate the sensitivity matrix $\mathbf{H}$, i.e., the matrix of partial derivatives of all measured quantities with respect to all parameters. A two-dimensional domain may be discretized into $\mathcal{O}(n_Y) \approx 10^4 - 10^5$ elements, with two parameters per element. Thus the computational effort of direct numerical differentiation would be prohibitive. Instead, we adopt the continuous adjoint state method, derived by *Sun and Yeh* [1990], to measurements of drawdown moments.

[35] Consider a particular step in the iteration procedure with the current estimates $\tilde{T}(\mathbf{x})$ and $\tilde{S}(\mathbf{x})$. First, we solve for the current estimates of the zeroth and the first temporal moments, $\tilde{m}_0(s_\delta(\mathbf{x}))$ and $\tilde{m}_1(s_\delta(\mathbf{x}))$, using the finite element method (FEM). Subsequently, we solve for a set of adjoint state equations for each measurement. In the following, $\mathbf{x}_\ell$ denotes the measurement location, $k \in [0, 1]$ is the index for the type of measurement, whereas ψ_1 and ψ_0 are the adjoint states of the first and zeroth moment, meeting the adjoint state equations:

$$-\nabla \cdot (\tilde{T}\nabla\psi_1) = \delta_{k1}\delta(\mathbf{x} - \mathbf{x}_\ell), \tag{20}$$

$$-\nabla \cdot (\tilde{T}\nabla\psi_0) = \delta_{k0}\delta(\mathbf{x} - \mathbf{x}_\ell) + \tilde{S}\psi_1, \tag{21}$$

subject to the boundary conditions:

$$\psi_i = 0 \quad \text{on} \quad \Gamma_{Diri}, \tag{22}$$

$$\mathbf{n} \cdot \nabla\psi_i = 0 \quad \text{on} \quad \Gamma_{Neu}, \tag{23}$$

for both $i = 0$ and $i = 1$.

[36] Subsequently, the sensitivity densities of the kth moment measured at $\mathbf{x}_\ell$ with respect to the log transmissivity $Y(\mathbf{x})$ and log storativity $Z(\mathbf{x})$ at location $\mathbf{x}$ are computed by

$$\frac{\partial m_k(\mathbf{x}_\ell)}{\partial Y(\mathbf{x})} = -\nabla\psi_0(\mathbf{x}) \cdot (\tilde{T}(\mathbf{x})\nabla\tilde{m}_0(\mathbf{x})) - \nabla\psi_1(\mathbf{x}) \cdot (\tilde{T}(\mathbf{x})\nabla\tilde{m}_1(\mathbf{x})), \tag{24}$$

$$\frac{\partial m_1(\mathbf{x}_\ell)}{\partial Z(\mathbf{x})} = \psi_1(\mathbf{x})\tilde{S}(\mathbf{x})\tilde{m}_0(\mathbf{x}). \tag{25}$$

[37] Since we consider the parameters to be uniform within elements, the sensitivity densities in equations (24) and (25) need to be integrated over the volume of the respective element. In the FEM context the temporal moments and adjoint states are defined at nodes, and the sensitivities have the form $\hat{\psi}_i^T\mathbf{M}\hat{\mathbf{m}}_j$, in which quantities with a hat are vectors of node-related values, and the matrix $\mathbf{M}$ is an element-related storage matrix for the sensitivity with respect to log storativity, and an element-related mobility matrix for the sensitivity with respect to log transmissivity.

[38] In summary, we arrive at the following procedure for the computation of sensitivities.

[39] 1. In case of a measurement of the zeroth temporal moment, ψ_1 is zero throughout the domain. A single adjoint pde of ψ_0, equation (21), needs to be solved. This equation is identical to a steady state groundwater flow equation with a point-like extraction at the observation point. A measurement of $m_0(s_\delta(\mathbf{x}))$ is insensitive to storativity, whereas its sensitivity with respect to log transmissivity can be computed for each element by integrating equation (24) over the element.

[40] 2. In case of a measurement of the first temporal moment, both adjoint state variables, ψ_1 and ψ_0, must be computed. First, one solves for ψ_1 by equation (20), which is a steady state groundwater flow equation with a point-like extraction at the observation point. Subsequently, one solves for ψ_0 by equation (21). This is a steady state groundwater flow equation with a distributed source term. The sensitivities with respect to log transmissivity Y and log storativity Z can be computed for each element by integrating equations (24) and (25) over the element.

5. Application to Synthetic Data

[41] To test our approach, we apply it to a series of artificially generated numerical test cases which differ in the spatial distribution of storativity.

5.1. Model Assumptions

[42] Our test cases represent two-dimensional, confined aquifers. The variability of drawdown with depth is neglected, so that equations (2) and (12) apply. For convenience, the model domain is assumed rectangular, with a fully penetrating well in the center of the domain. The boundary conditions are either of the Dirichlet or Neumann type, resulting in no drawdown or no flux, respectively.

[43] Over the past two decades, the fields of log transmissivity and hydraulic conductivity have been characterized intensively at various sites by geostatistical methods [e.g., *Rubin*, 2003, Tables 2.1 and 2.2]. To the best of our knowledge, a geostatistical characterization of the (specific) storativity, or its logarithm, has been done much less frequently. Typically, only a range of storativity values has been reported, for example, 10^{-6} to 10^{-3} for confined,

Table 1. Geometric Parameters and Pumping Conditions of All Test Cases, Geostatistical Parameters of Log Transmissivity, and Log Storativity in the Base Case

Parameter	Definition	Value
	Geometric Parameters	
L_1	domain length	1000 m
L_2	domain width	500 m
Δx_1	grid spacing in x_1	10 m
Δx_2	grid spacing in x_2	5 m
	Pumping Conditions	
Q	pumping rate	$4 \times 10^{-3}\,\mathrm{m^3/s}$
$x_{1,w}$	well coordinate	500 m
$x_{2,w}$	well coordinate	250 m
	Geostatistical Parameters	
σ_Y^2	prior variance of $\ln(T)$ [T in m²/s]	1
	actual variance of $\ln(T)$	0.89
σ_Z^2	prior variance of $\ln(S)$	1
	actual variance of $\ln(S)$	0.67
β_Y^*	prior mean value of $\ln(T)$ [T in m²/s]	−6
β_Z^*	prior mean value of $\ln(S)$	−9
$\sigma_{\beta_Y}^2$	prior variance of β_Y^*	1
$\sigma_{\beta_Z}^2$	prior variance of β_Z^*	1
λ_1^Y	correlation length in x_1 for $\ln(T)$	200 m
λ_2^Y	correlation length in x_2 for $\ln(T)$	100 m
λ_1^Z	correlation length in x_1 for $\ln(S)$	200 m
λ_2^Z	correlation length in x_2 for $\ln(S)$	100 m
	Measurement Error	
σ_s^2	variance of drawdown measurement	$4 \times 10^{-6}\,\mathrm{m^2}$

or 0.03 to 0.3 for unconfined aquifers [e.g., *Thorkildsen and Price*, 1991]. *Knowles et al.* [2004] stated that storativity ranges from 5×10^{-5} to 5×10^{-3} in confined aquifers. Two orders of magnitude is a typical range reported in textbooks for confined sedimentary aquifers [e.g., *Weight and Sonderegger*, 2000, Table 3.5]. *Sun et al.* [1995] examined the specific storage coefficients associated with different kinds of geological materials, finding an overall factor of 20 between the smallest and largest values. One of the few geostatistical inverse modeling studies estimating the spatial distribution of storativity from field data was performed by *Hendricks Franssen et al.* [1999], who analyzed data from the WIPP site. These authors obtained a variance of the log storativity of 1.78. In test cases with artificial data, much smaller values were assumed [e.g., *Zhu and Yeh*, 2005]. Thus, at the given state of knowledge, it is unclear which value the variance of log storativity has in a typical formation. In the following, we will use a value of unity.

[44] The studies of *Botha and Cloot* [2004] indicate that hydraulic conductivity and specific storativity are independent parameters. For the depth-integrated quantities, transmissivity and storage coefficient, a slight correlation is given via the thickness of the aquifer. Nonetheless, because there is no field evidence, we treat those two parameter fields as uncorrelated quantities.

5.2. General Setup

[45] All test cases are based on two-dimensional fields within rectangular domains. The parameters are defined on a regular grid, facilitating the application of spectral methods for the evaluation of cross covariances [*Nowak et al.*, 2003]. The field dimensions, grid spacing and pumping conditions are listed in Table 1. An extraction well with

pumping rate Q is located at $\mathbf{x}_w$. No flow is assumed across the top and bottom boundaries, whereas the head is fixed at the left- and right-hand side boundaries, the latter resulting in a fixed drawdown of zero according to equation (4).

[46] The fields of log transmissivity $Y = \ln(T)$ and log storativity $Z = \ln(S)$ are generated using the spectral method of *Dietrich and Newsam* [1993]. We use the nonseparable exponential covariance function for the fluctuations of both $\ln(T)$ and $\ln(S)$, together with a uniform, but uncertain prior mean, i.e., $X_Y(\mathbf{x}) = X_Z(\mathbf{x}) = 1$. The values of the geostatistical parameters are summarized in Table 1. Here, β_Y^* and β_Z^* are the uncertain prior mean values of the scalar drift coefficients for $\ln(T)$ and $\ln(S)$, whereas $\sigma_{\beta_Y}^2$ and $\sigma_{\beta_Z}^2$ are the corresponding prior variances, quantifying the uncertainty of β_Y^* and β_Z^*. The variances $\sigma_{\beta_Y}^2$ and $\sigma_{\beta_Z}^2$ form the diagonal elements of $\mathbf{Q}_{\beta\beta}$, which has off-diagonal entries of zero. σ_Y^2 and σ_Z^2 denote the variances of $\ln(T)$ and $\ln(S)$ about their mean values, and λ_1 and λ_2 refer to the correlation length in x_1 and x_2 direction, respectively.

[47] Figures 2a and 2b display the fields of the generated hydrogeological parameters. The actual mean of the generated fields and the corresponding geometric means of T and S are listed in Table 2. While the targeted variances of $\ln(T)$ and $\ln(S)$ are unity, the actual values of the generated fields are 0.89 and 0.67, respectively. The stars in Figure 2 mark the location of the observation wells on a grid of $x = 15$ m, 32 m, 50 m, 67 m, 85 m and $y = 5$ m, 15 m, 25 m, 35 m, 45 m. The pumping well, indicated by a square, is at the center point of the field.

5.3. Base Case

[48] On the basis of the "true" hydraulic parameters, we solve the transient groundwater flow equation using the Finite Element Method in space and central differentiation in time. A continuous pumping regime is assumed. Transient drawdown curves are recorded at the points marked by stars in Figure 2. Artificial measurement errors with zero mean and a standard deviation of 2 mm are added to the recorded values. These values are taken as measurements of transient drawdown. On the basis of these curves, we compute the normalized zeroth temporal moments $m_0(s_\delta(\mathbf{x}_\ell))$ and the characteristic times $m_1(s_\delta(\mathbf{x}_\ell))/m_0(s_\delta(\mathbf{x}_\ell))$ according to equations (10) and (11), which we use as data for our inverse method.

[49] In the following, we consider that n_1 head observations are needed until steady state is reached. The value of n_1 differs between the various applications (see Table 2). Subsequently, we take $n_2 = 100$ measurements of steady state drawdown. Then, linearized uncertainty propagation yields the following identities for the variances $\sigma_{m_0(s_\delta)}^2$ and $\sigma_{m_1(s_\delta)}^2$, expressing the measurement error of $m_0(s_\delta(\mathbf{x}_\ell))$ and $m_1(s_\delta(\mathbf{x}_\ell))$, respectively, as well as the covariance $C_{m_0 m_1}$ among the measurements of zeroth and first moments at the same measurement location $\mathbf{x}_\ell$:

$$\sigma_{m_0(s_\delta)}^2 = \frac{\sigma_s^2}{n_2 Q^2}, \tag{26}$$

$$\sigma_{m_1(s_\delta)}^2 = \frac{\Delta t^2 \sigma_s^2}{Q^2}\left(n_1 + \frac{n_1^2}{n_2}\right), \tag{27}$$

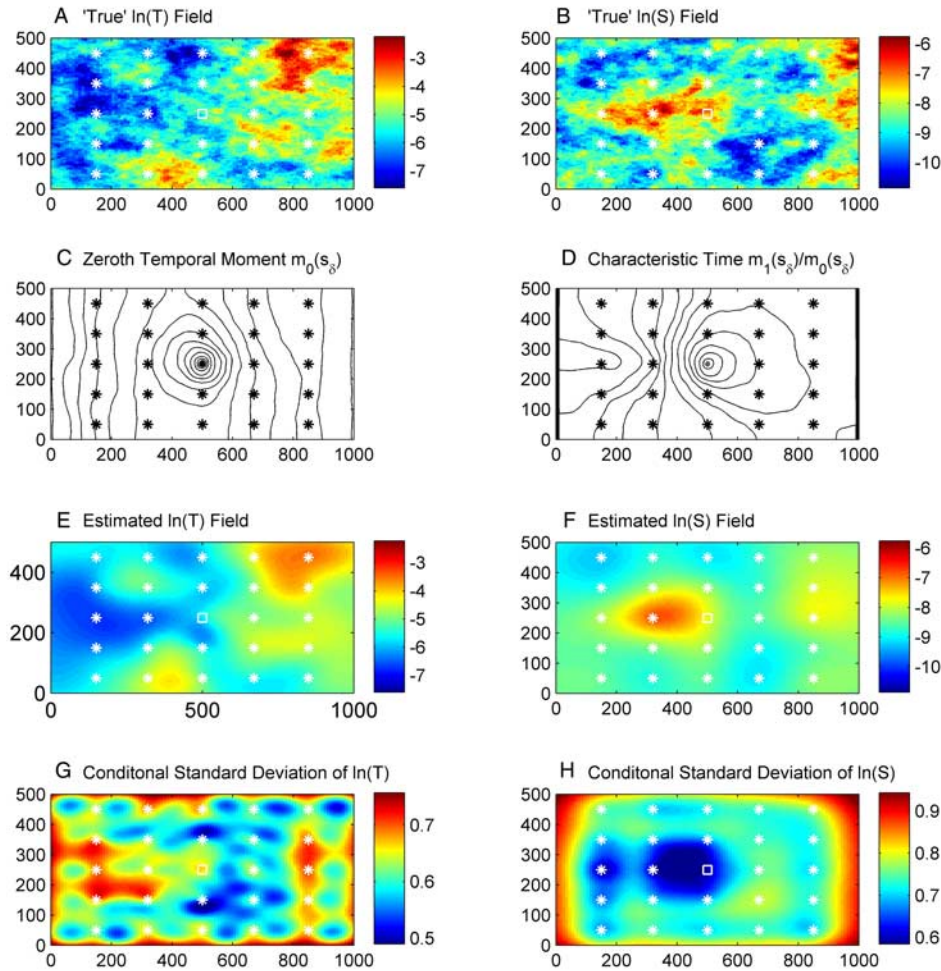$$C_{m_0 m_1} = -\frac{\Delta t}{Q^2}\sigma_s^2\frac{n_1}{n_2}, \tag{28}$$

Figure 2. "True" parameter fields, true distribution of zeroth temporal moment and characteristic time, estimated parameter fields of the base case, and their standard deviations of estimation. Contour levels are $\Delta m_0(s_\delta) = 12.5$ s/m^2 per line in Figure 2 (left) and $\Delta(m_1(s_\delta)/m_0(s_\delta)) = 500$ s per line in Figure 2 (right).

Table 2. Performance Criteria for the Various Test Cases[a]

	Definition	True	Base Case	Section 6.1	Section 6.2	Section 6.3	Section 7
n_1	number of time steps needed to reach steady state (10^4)		3.37	2.32	2.32	3.37	1.11
n_2	number of measurements in steady state		100	100	100	100	100
$\sigma^2_{m_0(s_\delta)}$	variance for measurement error of m_0 (10^{-3} s^2/m^4)		2.5	2.5	2.5	2.5	2.5
$\sigma^2_{m_1(s_\delta)}$	variance for measurement error of m_1 (10^6 s^4/m^4)		2.84	1.34	1.34	2.84	0.31
$C_{m_0 m_1}$	covariance for measurement error of m_0 and m_1 (s^3/m^4)		−84.11	−57.66	−57.66	−84.11	−27.59
β_Y	mean log tansmissivity (T in m^2/s)	−5.37	−5.32	−5.33	−5.28	−5.38	−5.12
T_g	geometric mean of transmissivity (10^{-3}m^2/s)	4.70	4.90	4.80	5.10	4.60	6.00
β_Z	mean log storativity	−8.62	−8.43	−8.63	−8.66	−8.21	−8.65
S_g	geometric mean of storativity [10^{-4}]	1.80	2.18	1.79	1.73	2.72	1.75
$\bar{\bar{\sigma}}_Y$	mean standard deviation of estimation for ln(T)	n.a.	0.62	0.53	0.64	0.60	0.62
$\bar{\bar{\sigma}}_Z$	mean standard deviation of estimation for ln(S)	n.a.	0.74	0.007	0.72	0.03	0.73
NRMSE(Y)	see equation (32) for ln(T)	n.a.	0.87	0.98	0.86	1.28	1.00
NRMSE(Z)	see equation (32) for ln(S)	n.a.	0.88	0.78	0.30	26.80	0.90
$r(Y)$	aliasing ratio for ln(T)	n.a.	n.a.	n.a.	3.4%	5.0%	n.a.
$r(Z)$	aliasing ratio for ln(S)	n.a.	n.a.	n.a.	2.4%	6.1%	n.a.

[a]True, realization shown in Figures 2a and 2b; base case, ln(S) correctly assumed spatially variable in the estimate; Section 6.1, ln(S) correctly assumed uniform in the estimate; Section 6.2, ln(S) erroneously assumed spatially variable; Section 6.3, ln(S) erroneously assumed uniform; Section 7, estimate using truncated drawdown curve; NRMSE, normalized root mean square error; n.a., not applicable.

in which σ_s^2 is the variance expressing the uncertainty of the drawdown measurements, whereas Δt is the size of the time steps. We consider no correlation of measurement errors between measurements at different locations. The values for $\sigma_{m_0(s_\delta)}^2$, $\sigma_{m_1(s_\delta)}^2$ and $C_{m_0 m_1}$ computed for the various test cases are listed in Table 2.

[50] Figures 2c and 2d show the distributions of the zeroth temporal moment, the characteristic time, and the location of the measurement points. In Figure 2c the difference in the zeroth temporal moments from one line to the next corresponds to 10 cm of steady state drawdown in the original pumping test with continuous extraction. In Figure 2d the difference in the characteristic time between two adjacent contour lines is 500s.

[51] With the artificially generated measurements of $m_0(s_\delta(\mathbf{x}))$ and $m_1(s_\delta(\mathbf{x}))$, we infer the distributions of $\ln(T)$ and $\ln(S)$ by the quasi-linear geostatistical approach of inverse modeling as described in section 3. For the given test case, 10 iterations are needed. The estimated parameter fields are shown in the Figures 2e and 2f. We use the same color scale for the true and estimated fields. In the following discussion, we refer to this test case, in which the correct geostatistical parameters are applied in the inverse method, as the base case.

[52] Besides the best estimate, the method also yields the estimation variance, quantifying the remaining uncertainty after conditioning. We display the conditional standard deviations of the estimate in Figures 2g and 2h. Table 2 contains the performance criteria for the various test cases. Here we list the estimated mean values of $\ln(T)$ and $\ln(S)$, the mean standard deviations of estimation for both parameters, and additional measures explained below.

[53] Comparing the true and estimated fields, Figures 2a versus 2e and 2b versus 2f, it is obvious that the estimate recovers the large-scale features, whereas the small-scale fluctuations are smoothed out. As seen in Table 2, the estimated mean transmissivity is slightly higher than the true value, whereas the estimated storativity is slightly smaller.

[54] Further studies (not shown) indicate that the method performs well for variances of the fields up to a value of 4. Because an increasing variance increases the degree of nonlinearity in the relationship between parameters and measured quantities, however, more iteration steps are needed.

5.4. Test of Unbiasedness

[55] With only a few locations of drawdown measurements, which are affected by measurement error, we do not expect that the estimated and true values of $\ln(T)$ and $\ln(S)$ agree perfectly. In the context of Bayesian analysis, the uncertainty of the estimate is expressed by the conditional covariance matrix $\mathbf{C_{pp|m}}$, as computed by equation (19). Our estimate is unbiased when the deviations between the true and estimated parameters, $\mathbf{p}_{true}$ and $\mathbf{p}_{est}$, have zero mean and covariance $\mathbf{C_{pp|m}}$:

$$E[\mathbf{p}_{true} - \mathbf{p}_{est}] = \mathbf{0}, \qquad (29)$$

$$E[(\mathbf{p}_{true} - \mathbf{p}_{est}) \otimes (\mathbf{p}_{true} - \mathbf{p}_{est})] = \mathbf{C_{pp|m}}. \qquad (30)$$

[56] We test this by performing two types of tests. In the first test, we consider only the estimation variance $\tilde{\sigma}_{p_i}^2$ of each parameter p_i, that is, the corresponding diagonal entry of $\mathbf{C_{pp|m}}$. We normalize $(\mathbf{p}_{true} - \mathbf{p}_{est})$ for each parameter by the standard deviation of estimation:

$$\varepsilon_{n,i} = \frac{p_{i,true} - p_{i,est}}{\tilde{\sigma}_{p_i}}, \qquad (31)$$

in which p_i is either the log transmissivity or log storativity in element i, and $\tilde{\sigma}_{p_i}^2$ is the estimation variance of that parameter.

[57] If our estimate of the conditional mean and variance is correct, the set of all normalized errors ε_n follows a standard normal distribution. We can summarize the overall error by the normalized root mean mean square error (NRMSE):

$$\text{NRMSE} = \sqrt{\frac{1}{n_Y} \sum_{i=1}^{n_Y} \varepsilon_{n,i}^2} \qquad (32)$$

[58] The normalized error ε_n, computed by equation (31), does not account for the conditional correlation of the parameters. We compute a vector of more accurate normalized errors ε_n^* by

$$\varepsilon_n^* = \mathbf{L}^{-1}(\mathbf{p}_{true} - \mathbf{p}_{est}), \qquad (33)$$

in which $\mathbf{L}$ is the Cholesky decomposition of the conditional covariance matrix $\mathbf{C_{pp|m}}$, that is, a lower triangular matrix meeting $\mathbf{LL}^T = \mathbf{C_{pp|m}}$. If the entries of ε_n^* follow a standard normal distribution, the computed conditional covariance matrix $\mathbf{C_{pp|m}}$ accurately describes the uncertainty about the estimate, including the correlation among the parameters.

[59] It is computationally more demanding to compute ε_n^* rather than ε_n, because for the former the full conditional covariance matrix $\mathbf{C_{pp|m}}$ must be evaluated and decomposed. Because of memory limitations, we have performed the full analysis only for a test case with reduced spatial resolution (50 $\times$ 50 elements). Figure 3 shows histograms of the diagonally scaled errors ε_n for $\ln(T)$ and $\ln(S)$, as well as the normalized error vector ε_n^* of all parameters accounting for conditional correlations. It is obvious that all three quantities follow a standard normal distribution, which is included in Figure 3 for reference. From this we conclude that our estimate is unbiased.

[60] For the original problem (100 $\times$ 100 elements), the values of NRMSE for $\ln(T)$ and $\ln(S)$ are listed in Table 2. They are close to the expected value of unity.

5.5. Reproduction of Drawdown Curves

[61] In the inverse model, we use the zeroth temporal moments m_0 and the characteristic time m_1/m_0 to summarize the most significant information conveyed by the transient drawdown curves. This raises the question, how much information is lost by disregarding all higher moments, such as the second to fourth central moments, which are related to the diffuseness, skewness, and kurtosis of the drawdown curves.

[62] In order to test the validity of restricting the analysis to the first two moments, we simulate transient drawdown curves using the true and estimated parameter fields of the
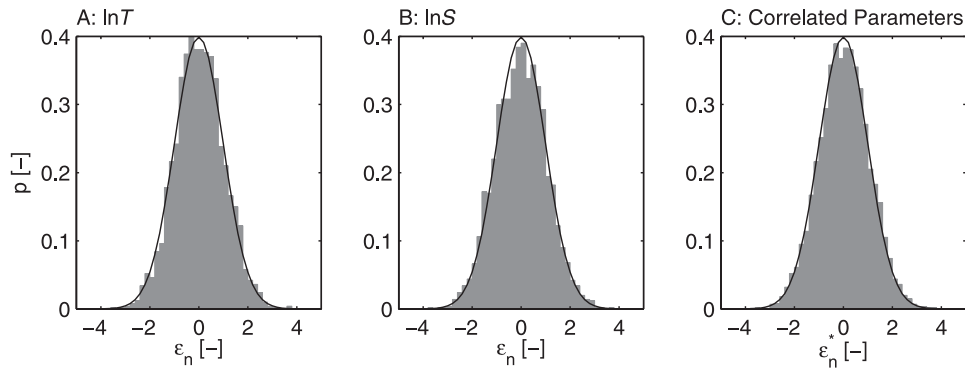
Figure 3. Distribution of normalized errors in a test case with coarser resolution. (A) Diagonally scaled error ε_n of the $\ln(T)$ field according to equation (31); (b) diagonally scaled error ε_n of the $\ln(S)$ field according to equation (31); (c) normalized error ε_n^* of all parameters accounting for conditional correlation among the parameters according to equation (33). Lines are standard normal distribution.

base case. Figure 4 shows these two drawdown curves in the observation well with the poorest match. The root mean square difference between the true and estimated transient heads in all wells is 1.3 mm, which is about 0.7 times of the measurement error. If we normalize the deviation of heads by the final drawdown of each observation well, we obtain a relative error of 0.3%. Therefore we conclude that the zeroth and first temporal moments are sufficient to characterize the transient drawdown curves in the inverse procedure. This is different to many solute transport applications, where process-specific tailing becomes obvious in higher-order moments of the breakthrough curve [e.g., *Harvey and Gorelick*, 1995b]. The main difference between solute transport and groundwater flow is that the pde of pressure head is strictly diffusive, whereas solute transport is dominated by advection. It may be possible, however, that higher-order moments of drawdown become more important in leaky than in confined aquifers.

6. Aliasing Between Transmissivity and Storativity

[63] As seen in equation (25), the sensitivity of the first temporal moment m_1 with respect to $\ln(S)$ is a function of the zeroth temporal moment m_0, which depends on the current estimate $\tilde{T}$. If $\tilde{T}$ is uncertain, then the sensitivity gives uncertain information on S. Likewise, the sensitivity of m_1 with respect to $\ln(T)$ depends on $\tilde{S}$. Because of these interdependencies, the estimated distributions of $\tilde{T}$ and $\tilde{S}$ depend on each other, and an error in one of them causes an error in the other. In this context, it is important to keep in mind that m_0 depends on the transmissivity only. Therefore a sufficient number of accurate measurements of m_0 will help to fix the estimate of $\ln(T)$, and the variability of m_1 measurements will correctly be attributed to the spatial variability of storativity. In many applications, however, the number of observation wells will be insufficient to fix the estimate of $\ln(T)$ rigidly.

[64] We refer to the misinterpretation of a particular parameter due to the uncertainty in another parameter as aliasing. As long as $\tilde{T}$ and $\tilde{S}$ are uncertain estimates, aliasing cannot be avoided. It will be the strongest when we base our estimate on wrong structural assumption about the parameters. In the following, we will focus on the assumptions

made for the storativity field. For this purpose, we perform three test cases: In section 6.1 the true $\ln(S)$ field is uniform, and we also estimate a uniform value; in section 6.2, the true $\ln(S)$ field is uniform, but we assume spatial variability of $\ln(S)$ in the estimation procedure; in section 6.3, finally, the true $\ln(S)$ field is spatially variable, but we estimate a uniform value.

[65] In the latter two cases, we analyze the deviation between the estimated values of $\ln(S)$ and $\ln(T)$ using the correct and wrong assumption regarding the spatial variability of storativity. We denote the root mean square deviation over the mean value, determined in the correct model, as aliasing ratio $r(p)$:

$$r(p) = \frac{1}{\beta_p^{est,corr.}} \sqrt{\frac{1}{n_Y} \sum_{i=1}^{n_Y} \left(p_i^{est,wrong} - p_i^{est,corr.} \right)^2} \quad (34)$$

in which p stands for the parameter (Y for log transmissivity and Z for log storativity), and the superscripts "wrong" and "corr." refer to the wrong or correct assumption about
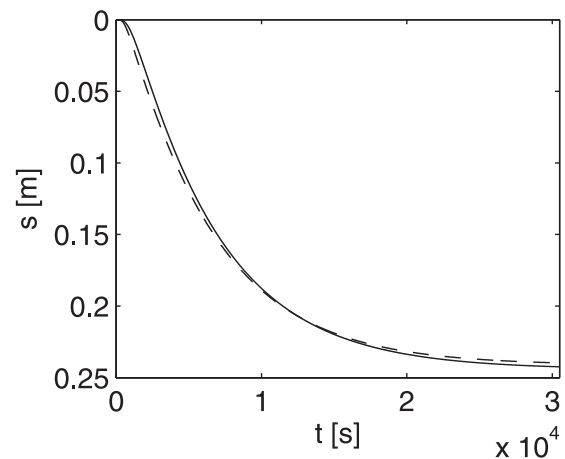

Figure 4. Comparison of transient drawdown curves applying the true and estimated fields at the observation well with the poorest match. Solid line shows true drawdown; dashed line shows drawdown based on the estimate using only temporal moments in the inversion.
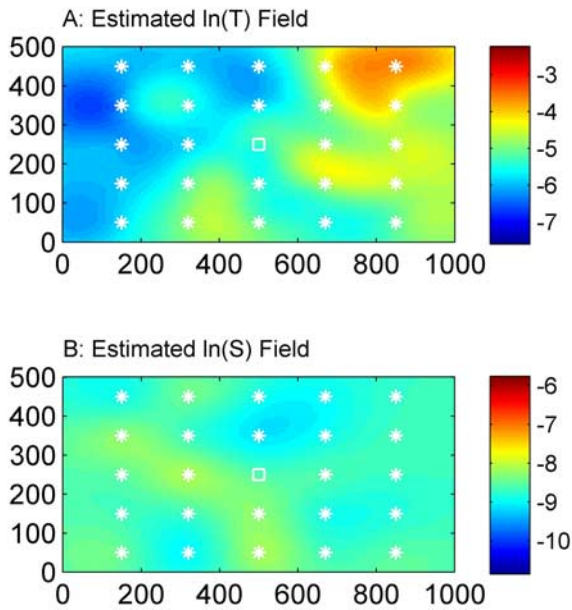
Figure 5. Estimated parameter fields in the test case assuming a spatially variable ln(S) field although the true field is uniform. Color scale is identical to Figures 2a and 2b.

the spatial variability of ln(S) in the inverse procedure. Values of $r(Y)$ and $r(Z)$ for various test cases are listed in Table 2.

6.1. Estimation With Constant ln(S)

[66] In this test case, we take the true ln(T) field of the base case (see Figure 2a). For storativity, we take a constant value, which is the geometric mean of the field used in the base case. After repeating the forward simulation and taking "measurements," we estimate a uniform value of ln(S) together with a spatially varying ln(T) field.

[67] In this test case, our prior knowledge about the storativity is strong. We know that ln(S) is uniform. This leads to an estimate of ln(S), which is close to the true value, and the corresponding estimation variance is very small (see Table 2). In practice, however, our prior knowledge regarding the storativity is limited. As discussed above, hydrogeological literature does not include many studies on the spatial variability of storativity. In the following, we test two limiting test cases: in the first we assume a spatially varying ln(S) field, although the true field is uniform. In the other test case we assume ln(S) to be uniform, although the true field is heterogeneous. In both cases we use the same ln(T) field as in the base case.

6.2. Aliasing Into ln(S)

[68] In this test case, the true ln(S) field is uniform. In the inverse procedure, however, we erroneously assume heterogeneity of the ln(S) field.

[69] Figure 5 shows the estimated fields. The estimate of ln(S) exhibits some fluctuations, although the true field was uniform. Obviously, parts of the variability observed in the measurements is mistakenly attributed to ln(S). As listed in Table 2, the aliasing ratio for ln(S) is 2.4% and for ln(T) 3.4%. From the statistical measures, it is practically impossible to determine that the estimate is based on

a wrong structural assumption concerning the variability of storativity.

6.3. Aliasing Into ln(T)

[70] In this test case, the true ln(S) field is that of the base case, thus exhibiting spatial fluctuations. In inversing, however, we erroneously assume that ln(S) is uniform.

[71] As listed in Table 2, the estimated uniform value of ln(S) is rather close to the mean value of the true field. The conditional standard deviation of the estimated uniform ln(S) value is much smaller than the spatial variability of the true field. The resulting NRMSE of the estimated ln(T) field is 1.28. That is, the true values of ln(T) deviate more strongly from the estimated values than expressed by the conditional variance. This finding indicates that the wrong structural assumption regarding the spatial variability of ln(S) impairs the estimate of the log transmissivity distribution, which is also expressed in the aliasing ratio for ln(T) of 5.0%. In practical applications, however, it may be difficult to determine the correct geostatistical parameters of ln(S). In results not shown here, we have tried to estimate the structural parameters of ln(S) from the data using the method of *Kitanidis* [1995]. In these attempts, we could sufficiently estimate the variance, but not the integral scales of the ln(S) fluctuations.

[72] In summary, both test cases using wrong structural assumptions about the spatial variability of storativity showed significant, but not dramatic deviations in the estimated log transmissivity fields.

7. Truncation of Drawdown Curves

[73] In practice, measurements of drawdown are prone to fluctuating errors. Consequently, the measured curves are not smooth. This poses difficulties to determine the time point at which steady state is reached. Truncating the drawdown curves too early will introduce a systematic measurement error and thus shifts the corresponding estimate. For demonstration purposes we perform a test with truncated measurements.

[74] In this test case, the time point at which the measurements are stopped is based on the rate of change of heads. If the maximal rate of change of drawdown in all monitoring wells is smaller than 2.4×10^{-6}m/s, we declare the process to have reached steady state and evaluate the "steady state" drawdown s_∞ from the next $n_2 = 100$ measurements of drawdown. Figure 6 shows the time point of truncation as a shaded vertical line, whereas the horizontal dashed line indicates the value of drawdown erroneously considered as steady state value. The corresponding zeroth temporal moment of Δh is calculated by integration from zero to the truncation time. From the final drawdown and $m_0(\Delta h)$, we compute $m_0(s_\delta)$ and $m_1(s_\delta)/m_0(s_\delta)$, according to equations (10) and (11).

[75] With these measurements of $m_0(s_\delta)$ and $m_1(s_\delta)/m_0(s_\delta)$, we perform our geostatistical inverse method. Plots of the estimated distributions of ln(T) and ln(S) (not shown) look rather similar to the estimates based on the extended time curves.

[76] As listed in Table 2, using the truncated measurements leads to slightly higher estimates of ln(T) and lower estimates of ln(S). These shifts reflect systematic errors caused by truncation: Both the final drawdown s_∞ and
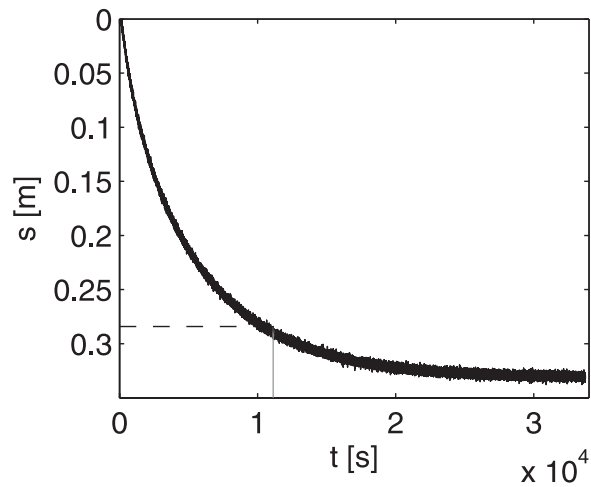
Figure 6. Transient drawdown curve with fluctuations due to measurement error. Shaded stripe shows time points, erroneously taken as steady state; dashed line shows final drawdown as determined from the truncated curve.

the characteristic time of drawdown $m_1(s_\delta)/m_0(s_\delta)$ are underestimated due to truncation. While, the true values are still within ± one standard deviation of the estimates, the systematic error is not accounted for in the estimation error, because the latter exclusively quantifies random deviation from the estimate.

[77] Nonetheless, because the shifts are rather small, we conclude that truncating drawdown curves in a responsible manner has only a minor impact on the estimate. In practice, other systematic errors, such as a wrong correction for atmospheric pressure fluctuations, may be more important.

8. Discussion and Conclusions

[78] We have successfully derived and implemented a new, computationally efficient method to identify transmissivity and storativity fields from transient drawdown curves obtained in pumping tests. We characterize the drawdown curves by their first two temporal moments. We have presented equations generating temporal moments of drawdown, which are formally identical to steady state equations. This leads to a dramatic reduction of computational costs in predictive modeling, in the evaluation of sensitivities, and thus in the overall inverse procedure. We have shown how the moments for a pulse-like extraction can be computed from measurements taken in pumping tests with continuous extraction or extraction over a time period.

[79] The concept of moment-generating equations has been introduced to subsurface hydrology by *Harvey and Gorelick* [1995b], who analyzed solute transport. In analogy to *Harvey and Gorelick* [1995a], *James et al.* [2000], and *Cirpka and Kitanidis* [2000], who used temporal moments of concentration in geostatistical inverse modeling, we use the temporal moments of drawdown. As inverse method, we have chosen the quasi-linear geostatistical approach of *Kitanidis* [1995]. Temporal moments of drawdown could also be considered in any other inverse method, both based on a geostatistical description of the parameter fields or a deterministic one. Replacing transient equations by a series

of steady state equations will reduce computational costs regardless of the inverse method chosen.

[80] We have restricted our analysis to the zeroth and first moment of a pumping-test with pulse-like extraction. We have shown that this restriction leads to acceptable results in the reproduction of transient drawdown curves. If even a better match is desired, the method can easily be extended to include higher-order moments. The moment-generating equation, equation (12), is not restricted to the zeroth and first moments, and extending the evaluation of sensitivities is straightforward. In practice, however, it may be difficult to obtain accurate measurements of higher-order moments.

[81] The pde of drawdown, equation (2), and the moment-generating equation derived from it, equation (12), require a clear separation between the drawdown induced by pumping and the natural hydraulic head. This is given when the heads are in steady state prior to pumping, and when the boundary conditions do not change in the course of the test. If these conditions are not met, the measurements of drawdown will become more uncertain, which has to be accounted for by larger values in the covariance matrix **R** expressing the measurement error.

[82] We have applied our method to two-dimensional confined aquifers. The method may also be applied to two-dimensional, depth-integrated flow in phreatic aquifers, described by the Boussinesq equation, if the thickness of the groundwater body is much larger than the drawdown. For shallow phreatic aquifers, the nonlinearity of the Boussinesq equation prohibits using the moment-generating equations.

[83] Extension to three dimensions is straightforward. Then, of course, the transmissivity is replaced by the hydraulic conductivity, and the storage coefficient by the specific storage coefficient. In our two-dimensional application, we assume that the Dupuit assumption holds, that is, flow is strictly oriented into horizontal directions and drawdown does not vary with depth. If the true flow field exhibits significant vertical components, e.g., in the vicinity of a partially penetrating well, a three-dimensional description will be needed. This restriction does not impart the applicability of moment-generating equations or the geostatistical approach of inverse modeling.

[84] Even though our model roots in a stochastic description of the aquifer properties, certain conceptual assumptions are deterministic. An example is the choice of boundary conditions. With the exception of the pumping rate in the well, most boundary conditions in practical applications are uncertain. In principle, it is possible to include parameters related to boundary conditions, such as leakage coefficients, in the set of parameters to be estimated, which we have not done in the current application. Thus, in practical applications the remaining uncertainty may be higher than in the given example. This uncertainty in the choice of boundary conditions, however, affects all inverse modeling schemes. It is unrelated to the question whether temporal moments are used as data or whether the aquifer parameters are characterized by geostatistics.

[85] Like in any application of geostatistical inverse modeling, the density of the observation wells must correspond to the integral scale of the formation. Our experience with test cases, not reported here, is that about one measurement per correlation length provides sufficient information to identify the unknown parameters within acceptable

error bounds. If the typical distance of wells is considerably larger than the integral scale, the obtained patterns of hydraulic parameters reflect the distribution of observation points rather than the true parameter distributions. If the largest distance of wells is considerably smaller than the integral scale, the estimated parameter fields correlate strongly. In such a case, fitting deterministic trend models may lead to equally good estimates of the parameter fields as geostatistical inverse methods.

[86] All relevant scales, that is, the "radius of influence" of the pumping test, the distance between the wells, and the integral scale of the heterogeneities, must match. As is evident from Figures 2g and 2h, the parameters can be estimated best in the direct vicinity of the extraction well. In order to infer parameters in large domains, it is thus necessary to combine results of several pumping tests using different wells for extraction. This technique is called hydraulic tomography [*Gottlieb and Dietrich*, 1995; *Yeh and Liu*, 2000]. Our approach to characterize transient head data by temporal moments may be applied to data from transient tomographic pumping tests, acting as an alternative to the steady shape analysis applied by *Bohling et al.* [2002], the ray-tracing technique of *Brauchler et al.* [2003], and the transient geostatistical approach by *Zhu and Yeh* [2005].

[87] Altogether, geostatistical inverse modeling of transient pumping tests using temporal moments of drawdown appears to be a promising technique for simultaneously identifying the spatial distribution of transmissivity and storativity. Its computational efficiency and robustness makes it possible to apply geostatistical inverse methods to transient pumping tests even if large computational domains are used.

References

Barrash, W., and M. E. Dougherty (1997), Modeling axially symmetric and nonsymmetric flow to a well with MODFLOW, and application to Goddard2 well test, Boise, Idaho, *Ground Water*, 35(4), 602–611.

Bohling, G. C., X. Zhan, J. J. Butler, and L. Zhang (2002), Steady shape analysis of tomographic pumping tests for characterization of aquifer heterogeneities, *Water Resour. Res.*, 38(12), 1324, doi:10.1029/2001WR001176.

Botha, J. F., and A. H. J. Cloot (2004), Deformation and the Karoo aquifer of South Africa, *Adv. Water Resour.*, 27(4), 383–398.

Brauchler, R., R. Liedl, and P. Dietrich (2003), A travel time based hydraulic tomographic approach, *Water Resour. Res.*, 39(12), 1370, doi:10.1029/2003WR002262.

Butler, J. J., and W. Z. Liu (1993), Pumping tests in nonuniform aquifers: The radially asymmetric case, *Water Resour. Res.*, 29(2), 259–269.

Certes, C., and G. de Marsily (1991), Application of the pilot point method to the identification of aquifer transmissivities, *Adv. Water Resour.*, 14(5), 284–300.

Cirpka, O. A., and P. K. Kitanidis (2000), Sensitivity of temporal moments calculated by the adjoint-state method and joint inversing of head and tracer data, *Adv. Water Resour.*, 24(1), 89–103.

DattaGupta, A., D. W. Vasco, and J. C. S. Long (1997), On the sensitivity and spatial resolution of transient pressure and tracer data for heterogeneity characterization, *SPE Form. Eval.*, 12(2), 137–144.

Dietrich, C. R., and G. N. Newsam (1993), A fast and exact method for multidimensional Gaussian stochastic simulations, *Water Resour. Res.*, 29(8), 2861–2869.

Gottlieb, J., and P. Dietrich (1995), Identification of the permeability distribution in soil by hydraulic tomography, *Inverse Probl.*, 11(2), 353–360.

Harvey, C. F., and S. M. Gorelick (1995a), Mapping hydraulic conductivity: Sequential conditioning with measurements of solute arrival time, hydraulic-head, and local conductivity, *Water Resour. Res.*, 31(7), 1615–1626.

Harvey, C. F., and S. M. Gorelick (1995b), Temporal moment-generating equations: Modeling transport and mass-transfer in heterogeneous aquifers, *Water Resour. Res.*, 31(8), 1895–1911.

Hendricks Franssen, H. J., J. J. Gomez-Hernandez, J. E. Capilla, and A. Sahuquillo (1999), Joint simulation of transmissivity and storativity fields conditional to steady-state and transient hydraulic head data, *Adv. Water Resour.*, 23(1), 1–13.

Hoeksema, R. J., and P. K. Kitanidis (1984), An application of the geostatistical approach to the inverse problem in two-dimensional groundwater modeling, *Water Resour. Res.*, 20(7), 1003–1020.

James, A. I., W. D. Graham, K. Hatfield, P. S. C. Rao, and M. D. Annable (2000), Estimation of spatially variable residual nonaqueous phase liquid saturations in nonuniform flow fields using partitioning tracer data, *Water Resour. Res.*, 36(4), 999–1012.

Kitanidis, P. K. (1995), Quasi-linear geostatistical theory for inversing, *Water Resour. Res.*, 31(10), 2411–2419.

Knowles, I., T. Le, and A. Yan (2004), On the recovery of multiple flow parameters from transient head data, *J. Comput. Appl. Math.*, 169(1), 1–15.

Kruseman, G. P., and N. A. de Ridder (1991), *Analysis and Evaluation of Pumping Test Data*, 2nd ed., Int. Inst. for Land Reclam. and Impr., Wageningen, Netherlands.

McLaughlin, D., and L. R. Townley (1996), A reassessment of the groundwater inverse problem, *Water Resour. Res.*, 32(5), 1131–1161.

Neuman, S. P., A. Guadagnini, and M. Riva (2004), Type-curve estimation of statistical heterogeneity, *Water Resour. Res.*, 40, W04201, doi:10.1029/2003WR002405.

Nowak, W., and O. A. Cirpka (2004), A modified Levenberg-Marquardt algorithm for quasi-linear inversing, *Adv. Water Resour.*, 27(7), 735–750.

Nowak, W., S. Tenkleve, and O. A. Cirpka (2003), Efficient computation of linearized cross-covariance and auto-covariance matrices of interdependent quantities, *Math Geol.*, 35(1), 53–66.

Oliver, D. S. (1993), The influence of nonuniform transmissivity and storativity on drawdown, *Water Resour. Res.*, 29(1), 169–178.

Rubin, Y. (2003), *Applied Stochastic Hydrogeology*, Oxford Univ. Press, New York.

Rubin, Y., and G. Dagan (1987), Stochastic identification of transmissivity and effective recharge in steady groundwater flow: 1. Theory, *Water Resour. Res.*, 23(7), 1185–1192.

Sanchez-Vila, X., P. M. Meier, and J. Carrera (1999), Pumping tests in heterogeneous aquifers: An analytical study of what can be obtained from their interpretation using Jacob's method, *Water Resour. Res.*, 35(4), 943–952.

Sun, N. Z., and W. W. G. Yeh (1990), Coupled inverse problems in groundwater modeling: 1. Sensitivity analysis and parameter identification, *Water Resour. Res.*, 26(10), 2507–2525.

Sun, N.-Z., and W. W.-G. Yeh (1992), A stochastic inverse solution for transient groundwater flow: Parameter identification and reliability analysis, *Water Resour. Res.*, 28(12), 3269–3280.

Sun, N. Z., M. C. Jeng, and W. W. G. Yeh (1995), A proposed gelogical parameterization method for parameter identification in three-dimensional groundwater modeling, *Water Resour. Res.*, 31(1), 89–102.

Thorbjarnarson, K. W., D. Huntley, and J. J. McCarty (1998), Absolute hydraulic conductivity estimates from aquifer pumping and tracer tests in a stratified aquifer, *Ground Water*, 36(1), 87–97.

Thorkildsen, D., and R. D. Price (1991), Groundwater resources of the Carrizo-Wilcox aquifer in the central Texas region, *Rep. 332*, Tex. Water Dev. Board, Austin.

Vasco, D. W., and S. Finsterle (2004), Numerical trajectory calculations for the efficient inversion of transient flow and tracer observations, *Water Resour. Res.*, 40, W01507, doi:10.1029/2003WR002362.

Vasco, D. W., H. Keers, and K. Karassaki (2000), Estimation of reservoir properties using transient pressure data: An asymptotic approach, *Water Resour. Res.*, 36(12), 3447–3465.

Weight, W. D., and J. L. Sonderegger (2000), *Manual of Applied Field Hydrogeology*, McGraw-Hill, New York.

Yeh, T.-C. J., and S. Liu (2000), Hydraulic tomography: Development of a new aquifer test method, *Water Resour. Res.*, 36(8), 2095–2105.

Yeh, T.-C. J., M. Jin, and S. Hanna (1996), An iterative stochastic inverse method: Conditional effective transmissivity and hydraulic head fields, *Water Resour. Res.*, *32*(1), 85–92.

Yeh, W. W. G. (1992), Systems-analysis in groundwater planning and management, *J. Water Resour. Plann. Manage.*, *118*(3), 224–237.

Zhu, J., and T.-C. J. Yeh (2005), Characterization of aquifer heterogeneity using transient hydraulic tomography, *Water Resour. Res.*, *41*, W07028, doi:10.1029/2004WR003790.

Zimmerman, D. A., et al. (1998), A comparison of seven geostatistically based inverse approaches to estimate transmissivities for modeling advective transport by groundwater flow, *Water Resour. Res.*, *34*(6), 1373–1413.

————————————

O. A. Cirpka and W. Li, Swiss Federal Institute of Aquatic Science and Technology (EAWAG), Überlandstrasse 133, CH-8600 Dübendorf, Switzerland. (olaf.cirpka@eawag.ch; wei.li@eawag.ch)

W. Nowak, Institut für Wasserbau, Universität Stuttgart, Pfaffenwaldring 61, 70550 Stuttgart, Germany. (wolfgang.nowak@iws.uni-stuttgart.de)